LBL-27690

Lawrence Berkeley Laboratory
UNIVERSITY OF CALIFORNIA

Presented at the 24th Rencontre de Moriond on
Nuclear Effects, Ion Collisions, and the Quark-Gluon Plasma,
Les Arcs, France, March 13–18, 1989

Physics with Nuclei at High Energies

W.M. Geist

August 1989

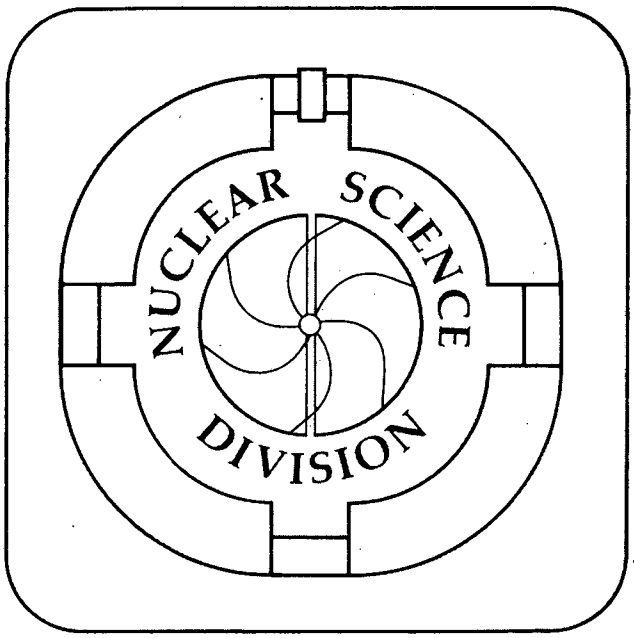

Prepared for the U.S. Department of Energy under Contract Number DE-AC03-76SF00098.

DISCLAIMER

PHYSICS WITH NUCLEI AT HIGH ENERGIES *

W. M. GEIST
Nuclear Science Division
Lawrence Berkeley Laboratory
1 Cyclotron Road
Berkeley, California 94720

Abstract :

Physics with nuclei at high energy is not reducible to a superposition of interactions involving individual nucleons; rather, qualitatively new phenomena show up. This is what one concludes from recent data on dilepton production off nuclei and on elastic proton-nucleus scattering. Furthermore, recent analyses of ion collisions at BNL and CERN reveal a number of non-conventional features. The relevant contributions to this Rencontre are summarized here.

* Summary talk on nuclear effects, ion collisions and the quark-gluon plasma, 24th Rencontre de Moriond, Les Arcs, March 1989.

I. Introduction

For quite some time nuclear targets were basically used only to enhance rates for rare high energy reactions, such as the Drell-Yan process or particle production at high transverse momentum. However, in the course of some experiments subtle nuclear effects were discovered (EMC effect [1], Cronin effect [2]). More recent efforts focus on the creation of "macroscopic" dense hadronic matter in ion collisions at high energy. This may lead to a phase transition to a deconfined plasma of quarks and gluons. A deeper understanding of strong interactions is sought in this way which is complementary to the approach based upon perturbative parton processes. The new data on nuclear effects contributed to this Rencontre are presented here.

II. Constituents of the Nucleus

While classical nuclear physics deals with nucleons as the fundamental building blocks of nuclei, the interest in the role of partons as constituents of nuclei is of more recent origin. Structure functions of partons have been derived from deep inelastic scattering of leptons off nuclei and protons. The remarkable finding was that quarks with small values of Bjorken x are suppressed in nuclei relative to free nucleons [1] . Similarly, one can determine, e.g., the structure function of antiquarks in nuclei A from a measurement of the Drell-Yan process in pA collisions (for quarks, see ref. [3]). Experiment E772 has obtained first results from p D and p Ca collisions at 800 GeV/c [4]. For dilepton masses $M \approx \sqrt{x_1 \cdot x_2 \cdot s} > 4$ GeV and $x_F = x_1 - x_2 > 0$ the data in fig. 1 were derived, i.e. the relative dimuon yields for Ca and D targets as function of Bjorken x of the antiquark, x_2 ; x_1 refers to a quark. Quite unexpectedly, an enhancement is found at $x_2 \leq 0.075$ for the heavier target. This is clearly different from the suppression of quarks first observed by the EMC collaboration [1] and awaits experimental corroboration and theoretical understanding.

III. Propagation of hadronic probes through nuclei

It is well know that hadrons are strongly absorbed in nuclei; hence the inelastic cross section is proportional to the nuclear surface: $\sigma_{in} \sim 4\pi R_A^2 \sim A^{2/3}$.

One may assume [5] that, e.g., a proton is a superposition of a large (L) and a small (S) parton configuration. These configurations may be subject to different reaction mechanisms described by two amplitudes F_L and F_S , respectively. For elastic pp scattering one has therefore $d\sigma/dt \sim |F_S + F_L|^2$; t is the Mandelstam variable. The experimentally observed [6] oscillatory pattern of $d\sigma/dt$ at 90^o as

function of $\sqrt{s}$ is compatible with an interference term expected in this framework. A nucleus could absorb the large proton configuration ($\sigma_{in} \sim A^{2/3}$), while it may be transparent to the small configuration of a size proportional to $1/\sqrt{|t|}$. For elastic scattering at 90^0 one has s/t = const. The "transparency" $T_A(s) = [d\sigma(pA \rightarrow pp\,(A-1))/dt] / [A \cdot d\sigma(pp \rightarrow pp)/dt]$ may therefore approach, with increasing $\sqrt{s}$, the limit $|F_S|^2 / |F_S + F_L|^2$. It should then exhibit the inverse of the oscillatory pattern of $d\sigma(pp \rightarrow pp)/dt$. The data in fig. 2 obtained by experiment E834 at BNL agree with this expectation [6]. It is worth mentioning in this context that an excellent suppression of non-elastic events was achieved by a precise measurement of both outgoing protons.

Based upon this success of the theory it is suggested in [5] to use nuclei in exclusive reactions to filter out non-perturbative phenomena, which are supposed to dominate F_L.

Next, propagation of pointlike probes through nuclei is considered. In the framework of QCD most quark and gluon scattering processes exhibit a pole at $t = 0$. It is therefore more economic to produce large angle partons by multiple small angle parton-parton scattering in nuclei rather than by a single large angle encounter. In the cases, where the large angle partons fragment into particles h with high transverse momentum p_T, this gives rise to the "Cronin-effect" : $d\sigma(pA \rightarrow h)/dp_T^2 \sim A^{\alpha}$, $\alpha \geqq 1$ for $p_T \geqq 1.5$ GeV/c [2] . Experiment E772 has obtained evidence for a similar effect from the Drell-Yan process and from J/ψ production in pD and pCa collisions [4]. In fig. 3 the ratio of yields normalized by A (A = D, Ca) exceeds unity for $p_T \geqq 2$ GeV/c. This feature tends to be more pronounced for J/ψ production. Presumably, initial state multiple scattering is stronger for gluons ($\sigma(gq) > \sigma(qq)$) which are at the origin of J/ψ. Also the J/ψ mesons may scatter elastically in the final state while dileptons remain essentially unaffected.

In conclusion, one finds that the response of nuclei to hadronic probes is given by a power α of A, which reflects the size of the probe : $\alpha \approx 2/3$ for hadrons, $\alpha \approx 1$ for "mini" hadrons and $\alpha > 1$ from collective phenomena in the case of partons.

IV. Ion collisions at high energy

In nuclear collisions at high energy [7] very dense hadronic matter may be created, hopefully - for theoretical convenience - at least in thermal equilibrium. This bulk matter is then characterized by its temperature T, volume V, pressure P and

baryochemical potential μ ('Fermi energy') or, equivalently, net baryon density n_B. It is obviously of central importance to extract these quantities experimentally.

1) Temperature

Differential cross sections for the production of hadrons of mass m in hadron-hadron collisions are of an approximate Boltzmann shape : $d\sigma/dp_T^2 \sim e^{-bm_T}$, $m_T = \sqrt{m^2 + p_T^2}$ [8], suggesting a thermal origin with a temperature given by the slope parameter b [9]. Typically $T \approx 160$ MeV is obtained. Pion production in the lab rapidity interval $y = 2 \div 3$ in SS collisions at 200 GeV/c/N cannot be reproduced by a single temperature as shown in fig. 4 [10] . A good fit to the date requires two temperatures $T_1 = 61 \pm 12$ MeV and $T_2 = 160 \pm 15$ MeV, or incorporation of collective flow [11] as shown in fig 4. Note that a temperature determined this way usually corresponds to the "freeze-out" temperature T_f of freely escaping hadrons after some expansion and cooling of the initial dense matter.

There remain a few unresolved questions :

i) What is the origin of the "excess" particles at $p_T \leq 250$ MeV^2 (see also ref. [12]).
ii) How does the Cronin effect shape the distribution at $p_T \geq 1.5$ GeV/c ?
iii) Why should pion spectra be thermal anyway, since they are known [13] to be dominated by resonance decay ?

One concludes that even a "simple" distribution reveals quite some open problems.

2) Baryon density

The initial net baryon density may determine to a large extent the space-time evolution of dense hadronic matter. While on expects for beam momenta of a few GeV/c/N a nearly complete "stopping" of the incident nucleons, hence a large net baryon density n_B at $y_{cm} \approx 0$, n_B should be negligible for $y_{cm} \approx 0$ at much larger energies. Experiment NA35 has attempted to determine the rapidity density dN/dy of the net number of protons from SS collisions at 200 GeV/c/N [10]. The inclusive spectrum of negative particles is subtracted from the one from positive particles using the proton mass throughout. The pion yields cancel this way, since sulfur nuclei are isoscalar ; there may be an excess of K^+ over K^-, which is, however, neglected. The resulting rapidity distribution of the difference between protons and antiprotons is shown in fig. 5 ; it is compatible with a substantial proton density at $y_{cm} \approx 0$. Note that neutrons and lambdas contribute also to the total net baryon denstity [14].

3) Volume

In a purely geometrical picture both projectile and target nucleons are either participating in the reaction or remain unaffected spectators. The kinetic energy of the participants is partially converted into transverse energy E_T (see fig. 6, ref. [15]); the spectator nucleons keep their initial momenta. Hence both a measurement of E_T (or $n_{ch} \sim E_T/\langle p_T \rangle$), and of the energy E^o, measured close to the beam direction, reflect the number of participants, or, equivalently, the impact parameter. In other words, these experimental quantities are related to the transverse size of the interacting system of nucleons which is, in this framework, bigger or equal to the transverse size of the intial thermalized matter. As shown by experiment WA80 [15] E_T and E^o are strongly correlated ; the distributions are also well reproduced by superpositions of nucleon-nucleon collisions [16] such that the geometrical interpretation is supported by these data.

The longitudinal size of the interaction region cannot easily be derived independently of dynamical models describing the formation of thermalized matter. Estimates range from a Lorenz-contracted diameter of the target for the lower energies to an educated guess of a typical length $L = \tau_0 = 0$ (1fm) for baryon free thermalized matter at high $\sqrt{s}$. This question was considered in some detail in ref. [15] on the basis of resulting energy densities ε.

4) Energy density

For ideal, relativistic gases one has $P = \varepsilon/3$, where the energy density ε is given by the thermalized energy E occupying the volume V (see above) : $\varepsilon = E/V$. Ideally one should measure the energy of all secondary particles, except for spectator nucleons, i.e. $E = \int (dE / dy)\ dy$. Most experiments measure transverse energy, or charged multiplicities, over a certain range of lab-pseudo rapidity η. To obtain

$$E = \int \frac{dE_T}{d\eta} \frac{dE}{dE_T}\, d\eta$$

one has to rely on a model for dE / dE_T. Often, decay of an isotropic fireball is assumed ; this is equivalent to complete "stopping" of participants [17a]. A detailed study shows, however, that even the data in the BNL energy range are not compatible

with isotropy [17b]. A general analysis of energy densities at 200 GeV/c /N was presented in ref. [15], as function of the length of the interaction volume. For central collisions $\varepsilon \approx 1 \div 3.5$ GeV/fm^3 is typically found (fig. 7), a value which is compatible with what is expected for the formation of a quark-gluon plasma.

In this context, experiments with large acceptance in pseudorapidity η are important, such as those based upon emulsion techniques or Si-counters coupled to calorimeters [18]. From these measurements E can be derived in a more reliable way. In a recent paper the measured widths of $d\sigma / d\eta$ were analysed in the Landau hydrodynamical model [19]. To fit the data longitudinal expansion is needed, restricting the kinematic limit of E_T to about 65 % of the upper limit provided by isotropic "fireballs". At the same time one gets an initial longitudinal size of about 1.5 fm and an initial temperature $T_i = 2T_f \approx 360$ MeV. This results finally in an energy density $\varepsilon \approx 7$ GeV/fm^3, which exceeds the energy density ε_π of pions at T = 360 MeV substantially.

In conclusion it should be emphasized that it is imperative, but tedious, to derive the characteristics of equilibrated dense hadronic matter from experiment. Generally, but not without stretching theoretical assumptions, one arrives at rather large energy densities.

V). Search for the quark-gluon-plasma

At energy densities above about 2 GeV/fm^3 formation of a plasma of nearly free quarks and gluons (QGP) is predicted to occur [7]. Potential signatures should therefore reflect the existence of free partons at a typical temperature of about 200 MeV.

1) Electromagnetic probes

Thermal partons may produce photons or dileptons whose average (transverse) momenta and masses are in the order of the temperature. Detector and background problems may, however, require a study of the tails of the predicted distributions. The crucial advantage of these probes is negligible reinteraction with the surrounding hadronic phase.

Experiment NA34 has presented first results on production of dimuons with mass $M \geq 0.45$ GeV, $p_T \geq 0.2$ GeV/c and $y > 4.1$ from SA collisions at 200 GeV/c/N

[20]. Since the experiment is not optimized for dimuon detection in this kinematical range, the extraction of a "prompt" dimuon signal is difficult. An attempt was made to remove dimuons produced in the dump, and to correct for the remaining contribution from the dump ; also dimuons due to pion and kaon decays were subtracted. The final prompt dimuon signal in fig. 8 is compatible with the yield expected from conventional sources (ρ, ω, φ, η, η'). No evidence for an additional signal, neither from thermal partons, nor from the Drell-Yan process, nor from semileptonic decays of D-meson pairs [21] was found so far. This may be due to the small production angle ($y > 4.1$).

2) Strangeness

The QGP consists largely of gluons, due to their many degrees of freedom. These gluons produce a substantial abundance of strange quarks [22] presumably in chemical equilibrium. This feature should be especially pronounced for net baryon densities $n_B > 0$, since gluo-production of pairs of light quarks is suppressed by the Pauli principle. The most promising detectable signal of the large density of s and $\bar{s}$ quarks are supposed to be multistrange antibaryons which cannot easily be created in the competing scenario of a dense hadron gas. Strangeness production during hadronization and in the final gas of hadrons may modify the yields of strange hadrons from the QGP. A more detailed account of all these aspects and of analysis approaches is given in ref. [22].

Unexpected results on this subject were presented by experiment E802 performed with a Si beam of 14.5 GeV/c/N on gold targets [23]. For $1.2 \leq y \leq 1.5$ the differential cross sections for kaons and pions are given as function of m_T in fig. 9. The measured K/π ratios [23] are larger than those derived from pp and pPb collisions; furthermore K^+ are more abundantly produced than K^- by a factor of about 4, and both yields exceed Fritjof predictions [23]. While the data may be compatible with expectations from the QGP, also a hadron gas may produce K^+ abundantly, e.g., by the reaction $\pi N \rightarrow K^+ \Lambda$, whereas K^- may disappear due to the reaction $K^- N \rightarrow \pi \Lambda$. In this context one may also speculate about production and reabsorption of (strange) vector mesons.

In passing it should be noted that the relative yield of protons in this experiment is exceptionally large, and that the data extend out to the kinematic nucleon-nucleon limit.

Worth mentioning here is also another unusual phenomenon involving

strangeness. It is the dependence of the average number of Λ per event on the square of the charged multiplicity, measured for SS collisions by NA35 [24].

First results from experiment WA85 are very encouraging [25]. In addition to Λ and $\bar{\Lambda}$, clear signals of Ξ^- were seen for the first time in SW collisions at 200 GeV/c/N; backgrounds are small as demonstrated by fig. 10.

Additional information on strange (anti-) baryons should be provided soon by experiment NA36 who obtained evidence for production of Λ in SPb collisions at 200 GeV/c/N up to the highest multiplicities [26]. A reconstructed TPC event including a clear V^0 is displayed in fig. 11 [27].

3) Suppression of J/ψ

The NA38 data on J/ψ suppression at 200 GeV/c/N are well known [28],29], hence only the main features are reported here.
1) In OU collisions the ratio of the number of J/ψ per central event ($E_T >$ 85 GeV) normalized to the continuum to the one for more peripheral events ($E_T <$ 34 GeV) increases from a value of about 0.40 at p_T(J/ψ) = 0 to about 1 at p_T (J/ψ) = 2.3 GeV/c. The data are reproduced in fig. 12.
2) The number of J/ψ normalized to the continuum decreases as a function of energy density for OU and SU collisions (fig. 13).

These trends may be a consequence of the dissolution of the binding due to the deconfining QGP. In this framework J/ψ mesons with higher (transverse) momenta spend less time in the QGP and are therefore suppressed less efficiently.

An exhaustive and clear exposition of current theoretical interpretations is presented in ref. [29], which can be summarized in the following way :

i) The data are consistent with an interpretation in the QGP framework. Parameters describing the QGP are taken from the experiment itself and are affected by non-negligible uncertainties. A typical model calculation is shown in fig. 14 [30a].

ii) Hadronic absorption models explain the level of J/ψ suppression satisfactorily, but generally do not reproduce the observed p_T dependence. Incorporation of initial state multiple parton scattering yields a more pronounced widening for the p_T distribution of J/ψ than for the dimuon continuum (see section III). This resembles then a p_T dependent suppression factor as illustrated in fig.15 [30b].

These models depend critically on the way cross sections for J/ψ-hadron collisions are extracted from photoproduction experiments [29].

It is interesting to note that also in the hadron gas model one has to assume high density matter to achieve the absorption measured.

On an even more fundamental level it was argued that a correct quantum mechanical treatment may give results differing from those based upon classical quark trajectories [31].

Hopefully, one may be able to distinguish between the two main classes of models by extending the measurements to higher p_T and lower energy densities. At $p_T > 2$ GeV/c the ratio shown in fig. 12 should stay constant in case of QGP formation : the J/ψ mesons do not stay long enough in the QGP to feel any effect. Initial state parton scattering, on the other hand, affects p_T distributions over the whole accessible p_T range, such that the relevant ratio (fig. 12) should continue to grow beyond $p_T \approx 2$ GeV/c.

When lowering the energy density below the threshold for QGP formation, deconfining effects should cease, such there is no more dependence on ε of the normalised number of J/ψ (fig. 13). In hadronic absorption models a continuous increase is predicted.

Low energy densities can be achieved either at constant beam momentum, by going to larger impact parameters, or by lowering the beam momentum at fixed impact parameter. The latter approach assures a constant number of participants, such that trivial nuclear effects ('A-dependence') are excluded.

At much higher energies there may even be a potential enhancement of J/ψ production, at least in the model of ref. [32], due to J/ψ regeneration by the rather abundant χ-mesons. A recent measurement of χ production in pA collisions at 530 GeV/c is reported in ref. [33].

VI) Electromagnetic Process

Experiment E 814 measured peripheral OA collisions at 14.5 GeV/c/N [34]. Events were recorded where all incident projectile nucleons emerge with a

momentum very close to the initial one. The corresponding cross sections depend strongly on the charge Z_T of the target (fig. 16), whereas a proportionality to $A^{1/3}$ is found for inelastic peripheral collisions. Hence one has obtained additional evidence [35] for the occurence of electromagnetic projectile dissociation. The cross sections for these processes are of course expected to be proportional to Z_T^{β}, with β close to 2. At higher energies electromagnetic cross sections may exceed nuclear cross sections and become limiting factors of beam life-time.

The idea of electromagnetic interactions was recently applied to Higgs production in nuclear collisions at center-of-mass energies of a few TeV [36]. The Higgs particle may be produced in "2γ"-events at a reasonable rate, which is proportional to $Z_{Beam}^{2\beta}$. No other particles would be produced simultaneousy. Higher luminosities in $p\bar{p}$ colliders have to be balanced against backgrounds in both $p\bar{p}$ and AA collisions [37].

VII. Conclusions

One of the main topics of this Rencontre was the investigation of hadronic bulk matter occupying a 'macroscopic' region of space. This new field is particularly interesting since it may lead to a better understanding of the QCD vacuum, provided a phase transition to a Quark-Gluon Plasma occurs. First experimental results [12b] were already indicative of high energy densities and some non-trivial effects. Based upon the more recent data presented here a more detailed picture of the characteristics of dense matter begins to emerge. Inclusive distributions of transverse momenta, production of strangeness and of J/ψ mesons reveal non-trivial new features. This is a very encouraging situation.

A correct interpretation of these phenomena requires a thorough knowledge of pp and pA collisions, which are, of course, also interesting in their own right. Nuclear targets introduce a rather large spatial dimension into high energy processes such that collective effects and/or time dependence of hadron formation can be investigated. First results on the antiquark-sea in nuclei, on nuclear effects in dilepton production and elastic scattering underline this point. Finally, it is amusing to note that observation of a classical electro-magnetic dissociation in nuclear scattering obviously triggered ideas on Higgs production in nuclear collisions at LHC energies.

Acknowledgments

I am indebted to the organizers for inviting me to an interesting conference in a friendly and stimulating atmosphere; I profited much from discussions with many participants, especially with those whose results are summarized here.

This work was supported by the Director, Office of Energy Research, Office of High Energy and Nuclear Physics, Nuclear Physics Division of the U.S. Department of Energy under Contract DE-AC03-76SF00098

FIGURE CAPTIONS

Fig. 1 Ratio of differential cross sections for dilepton production by protons off Ca and D as function of Bjorken x of the antiquark (x_2).

Fig. 2 a) The transparency for Al at 90^o CM vs effective incident momentum.
b) The pp differential cross section scaled by s^{10}.

Fig. 3 a) see fig.1, but as function of p_T.
b) see a), but for J/ψ production.

Fig. 4 Transverse momentum distribution of pions in central S+S collisions at mid-rapidity. The solid line is a thermal fireball fit; the dashed line is the flow model.

Fig. 5 Rapidity distribution for "protons" in S+S collisions.

Fig. 6 Transverse energy distribution from 200-GeV/nucleon ^{16}O (circles) and ^{32}S (histograms) reactions with various target nuclei in the pseudorapidity range $2.4 < \eta < 5.5$. The sulfur data are preliminary.

Fig. 7 Energy density estimates by various methods for 200 GeV/nucleon ^{16}O- and ^{32}S-induced reactions as a function of the total thickness of the interacting system. The Pb + Pb points are based on an extrapolation of the observed E_T scaling.

Fig. 8 Comparison between experimental dimuon signal (- -) and known sources (—).

Fig. 9 Invariant cross section for π and K. The dashed curves are the result of FRITIOF calculations while the full lines are exponentials with a slope of 170 MeV. Note that the K^+ cross sections are multiplied by 0.1.

Fig. 10 Effective $\Lambda\pi^-$ mass distributions for cascade candidates.

Fig. 11 Example of 200 A GeV/c sulphur-lead interaction with an identified V^0 candidate observed in the NA36 TPC.

FIGURE CAPTIONS

Fig. 12 Ratio of the relative numbers, normalized to the continuum, of J/ψ mesons for central and peripheral oxygen- and sulphur-uranium collisions at 200 GeV/c/N as function of p_T (J/ψ).

Fig. 13 Ratio of the number of J/ψ mesons to the continuum, as function of energy density for pp, pU, OU and SU collisions at 200 GeV/c/N.

Fig. 14 Transverse-momentum dependence of the ratio of the acceptance functions,

$$R(p_T) \equiv \frac{A\ (p_T,\ E_{min},\ E_{max} = 80\ GeV)}{A\ (p_T,\ E_{min} = 0,\ E_{max} = 28\ GeV)},$$

for an oxygen beam at 200 GeV/nucleon compared to NA38 data points. The three solid curves correspond to calculations with E_{min} = 40, 50, 60 GeV, respectively. Also shown as a dashed curve are results assuming a static plasma.

Fig. 15 (a) The preliminary NA38 data on the relative J/ψ-to-continuum yield with $E_T^{>} > 85$ GeV and $E_T^{<} < 34$ GeV are compared to calculations for the analogous LUND model values $E_T = 60$ and 15 GeV including both quasielastic initial-state scattering and final-state inelastic J/ψ-hadron scattering. The dashed curve shows the suppression factor in the absence of initial-state interactions. (b) Transverse momentum distributions of p + A → ψ + X at 200 GeV for ^{195}Pt (diamonds) and p (squares) targets are compared to those measured in O+U (dots) for $E_T > 85$ GeV . The O+U curve is calculated for $E_T = 60$ GeV.

Fig. 16 Cross section for forward production of the nuclear systems indicated as function of the charge of the target for an oxygen beam at 14.5 GeV/c/N.

References

[1] J.J. Aubert et al.; Phys. Lett. 123B (1983) 275.

[2] J.W. Cronin et al., Phys. Rev. D 11 (1975) 3105.

[3] P. Bordalo et al.; Phys. Lett. 193B (1987) 368.

[4] P.L. Mc Gaughey, Study of the Nuclear Anti-quark Sea via $p + N \rightarrow \mu^+ \mu^- + x$, these proceedings.

[5] J.P. Ralston and B. Pire, Nuclear Filtering of Strong Interactions, these proceedings.

[6] A.S. Carroll, Investigation of Color Transparency by High Transverse Momentum pp Elastic Scattering inside Nuclei, these proceedings.

[7] W.M. Geist, Ultrarelativistic Nuclear Physics : From Becoming to Being, LBL 26286, to be published in Int. J. Mod Phys. A.

[8] K. Guettler et al., Nucl. Phys. B116 (1976) 77.

[9] R. Hagedorn, Rivista Nuov. Cim. 6 (1983) 10.

[10] D. Röhrich, Proton Spectra in Central Nucleus-Nucleus Collisions at CERN SPS Energies, these proceedings.

[11] see eg. U. Heinz et al., Univ. Regensburg preprint, TPR 89-13.

[12] a) H.G. Fischer, Z. Phys. C38 (1988) 105;
b) see also C.W. Fabjan, Proceedings, 23rd Rencontres de Moriond, Les Arcs, 13-19 March 1988.

[13] H. Grässler et al., Nucl. Phys. B132 (1978) ;
Y.A. Tarasov, Sov. J. Nucl. Phys. 42 (1985) 260.

[14] W.M. Geist, pp, pA and $\alpha\alpha$ collisions and the Understanding of the Quark-Gluon Plasma, Proceedings of the 23 nd Rencontre de Moriond, Les Arcs.

[15] T. Awes, Transverse Energy Scaling and Energy Density Estimates from O- and S- Induced Reactions, these proceedings.

[16] K. Werner, String Models for Ultrarelativistic Nuclear Collisions, these proceedings.

[18] M. Masera, Charged Particle Multiplicity in Heavy - Ion Collisions from the Helios Experiment, these proceedings.
G. Rosa, Ion Collisions Selected by E_T in Emulsion, these proceedings.

[19] F. Lamarche and C. Leroy, Longitudinal Expansion of Hadronic Matter at Large Energy Densities in Ultrarelativistic Nucleus-Nucleus Collisions, Mc Gill Univ. preprint.

[20] G. Vasseur, Low Mass Muon Pairs Production in Sulphur-Nucleus Collisions, these proceedings.

[21] H. G. Fischer and W.M. Geist, Z. Phys. C 19 (1983) 159.

[22] a) P. Koch et al., Phys. Rep. C 142 (1986) 167.
b) H.C. Eggers and J. Rafelski, Strange Particles and Quark Gluon Plasma in Nuclear Collisions : Current Status, these proceedings.

References

[23] F. Videback, Results from the BNL E802 Experiment with 14.5 GeV/c/u Si Beam, these proceedings.

[24] See eg. G. Odyniec, LBL-26728, Proceedings of the Conference on Hadronic Matter in Collision, Tucson, AZ, Oct. 1988.

[25] M.T. Trainor, Preliminary Results on Ξ^- Production at $P_T \geq 1$ GeV/c in the Central Rapidity Region in 200 GeV/c Sulphur-Tungsten Interactions, these proceedings.

[26] D. Greiner, LBL-26590, Proceedings of the Conference of Hadronic Matter in Collision, Tucson, AZ, Oct. 1988.

[27] NA36 Collaboration, private communication.

[28] C. Baglin, Phys. Lett. 220 B (1989) 471; P. Sonderegger, CERN-EP/89-19.

[29] R.A. Salmeron, The Suppression of J/ψ in High Energy Nucleus-Nucleus Collisions-Experimental Data and Models, these proceedings, and references there in.

[31] R.L. Thews, Comments on J/ψ Suppression and Quantum Mechanics, these proceedings.

[32] R. Vogt et al., Phys. Lett. 207B (1988) 263.

[33] K. De, Preliminary Results from Fermilab Experiment E672, these proceedings.

[34] E. O'Brien, Peripheral Interactions, these proceedings.

[35] D. Olson et al., Phys. Rev. C24 (1981) 1529 ;
J.C. Hill et al., Phys. Rev. Lett. 60 (1988) 999;
E. Andersen et al., Phys. Lett. 220B (1989) 328;
C. Brechtmann and W. Heinz, Z. Phys. A330 (1988) 407.

[36] E. Papageorgiu, MPI-PAE/PTh 23/88

[37] M. Drees et al., Phys. Lett. 223B (1989) 454.

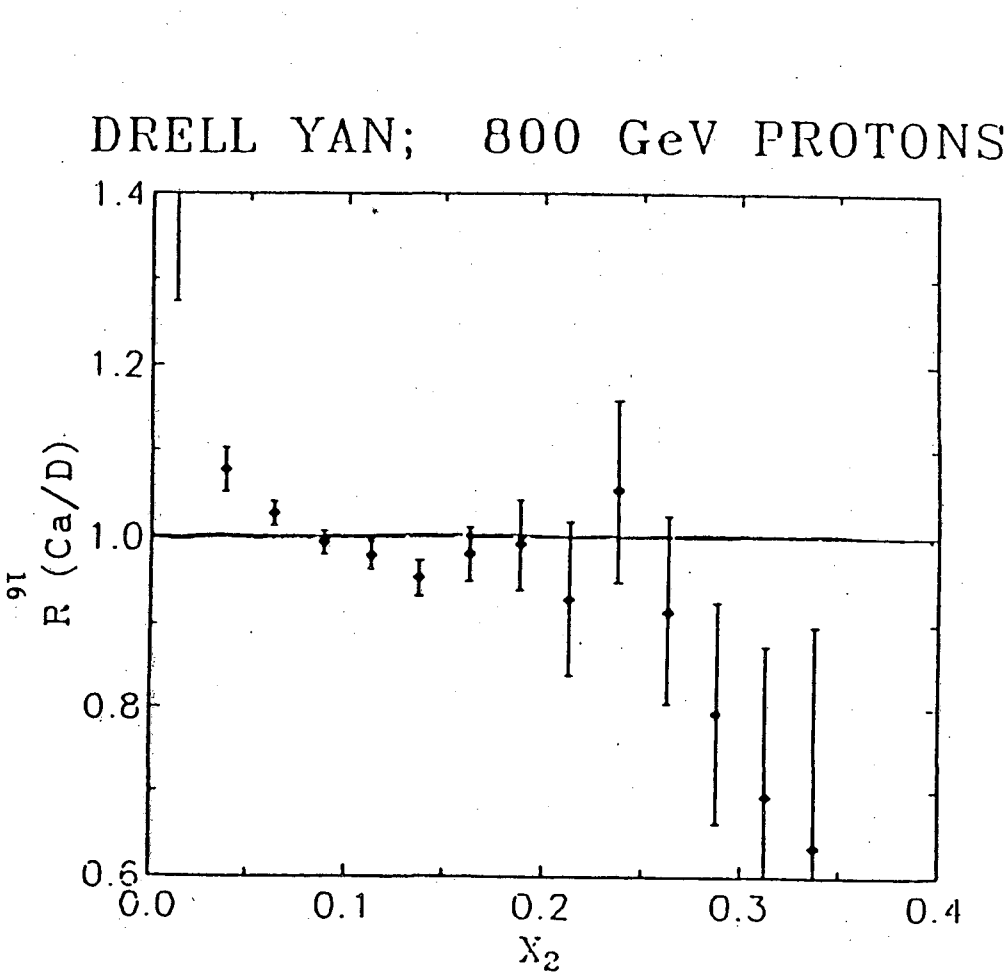
DRELL YAN; 800 GeV PROTONS
R (Ca/D)
^{16}
1.4
1.2
1.0
0.8
0.6
0.0
0.1
0.2
0.3
0.4
X_2

Fig. 1

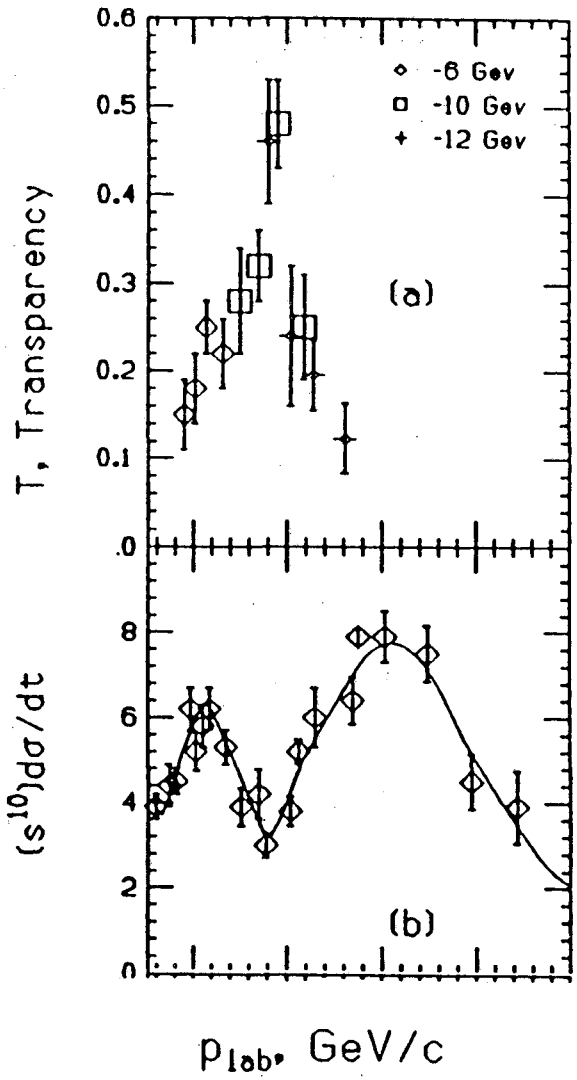
-6 Gev
-10 Gev
-12 Gev
T, Transparency
(a)
(b)
$(s^{10})d\sigma/dt$
p_{lab}, GeV/c

Fig. 2

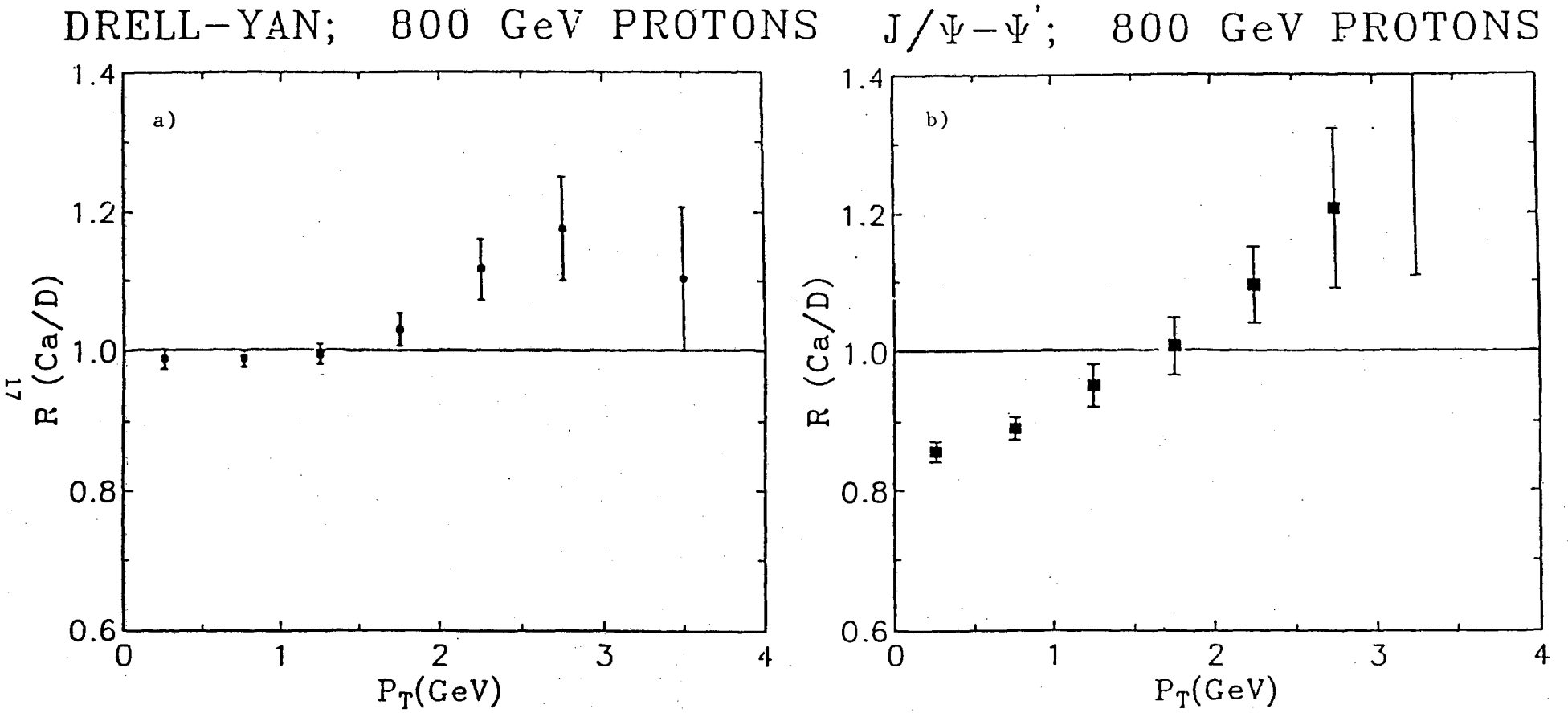
DRELL-YAN; 800 GeV PROTONS
J/Ψ-Ψ'; 800 GeV PROTONS
a)
b)
R (Ca/D)
P_T(GeV)
1.4
1.2
1.0
0.8
0.6
0
1
2
3
4

Fig. 3

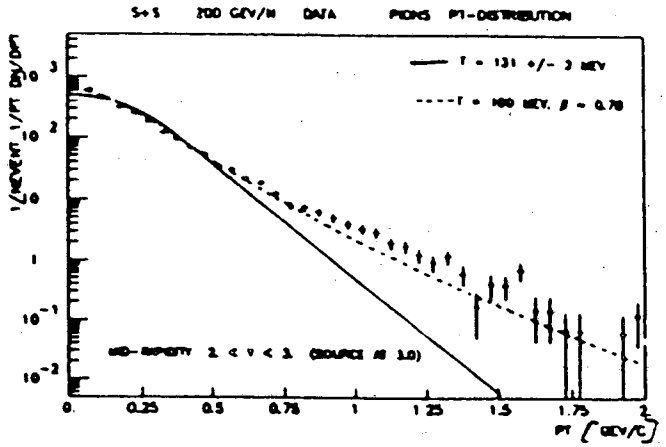

Fig. 4

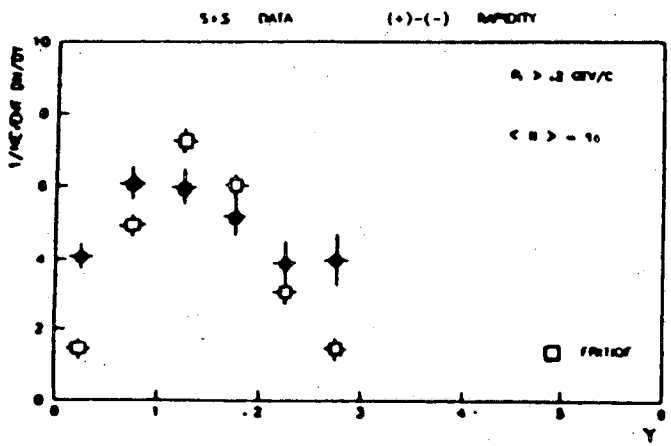

Fig. 5

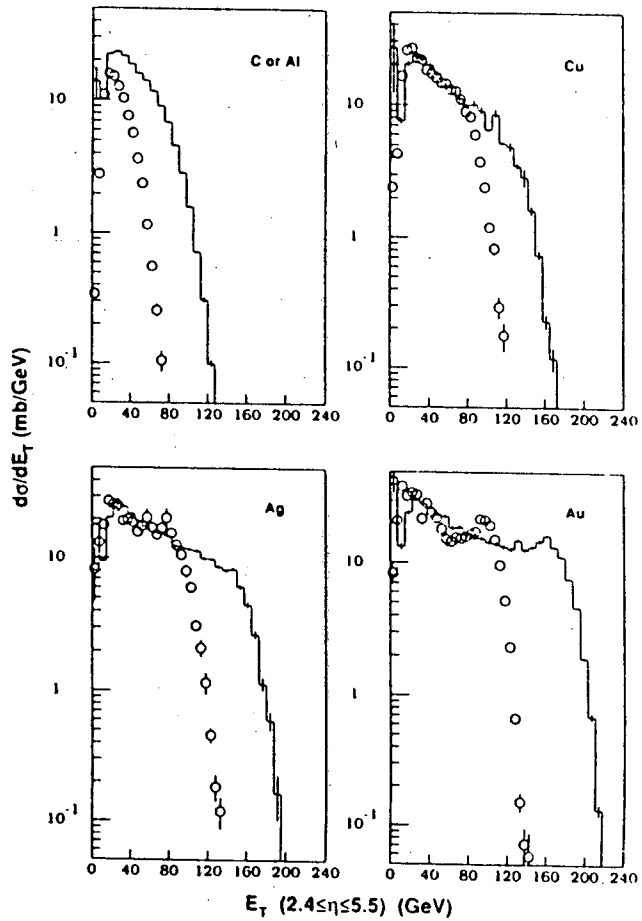

Fig. 6

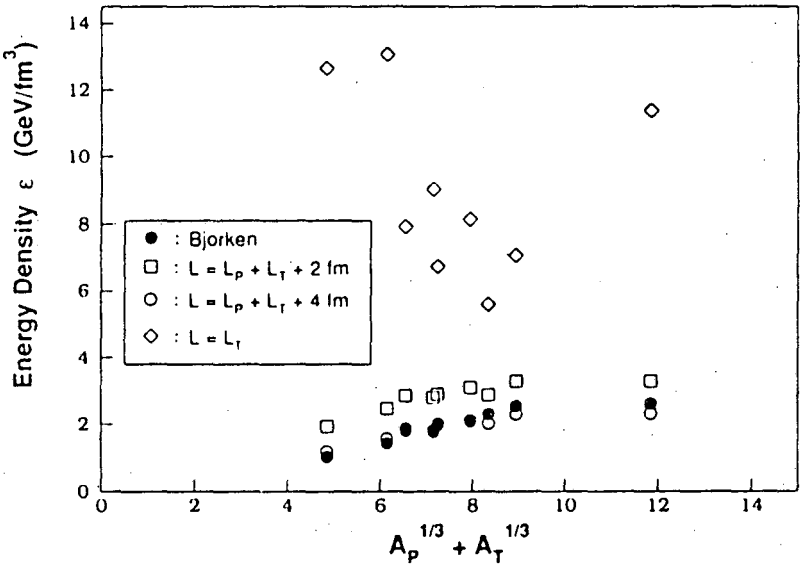
Energy Density ε (GeV/fm³)
: Bjorken
: L = L_P + L_T + 2 fm
: L = L_P + L_T + 4 fm
: L = L_T
A_P^1/3 + A_T^1/3

Fig. 7

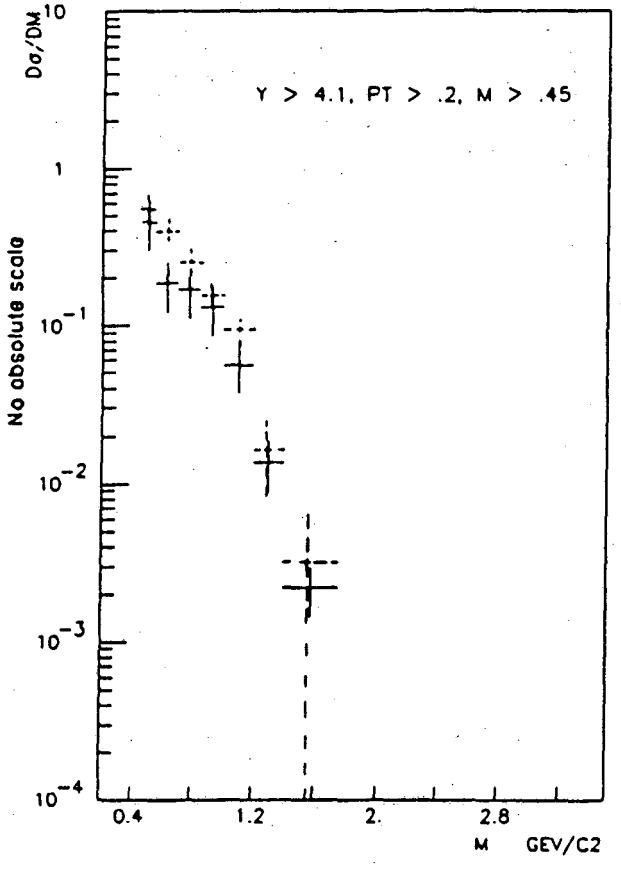
Dσ/DM
Y > 4.1, PT > .2, M > .45
No absolute scale
M GEV/C2

Fig. 8

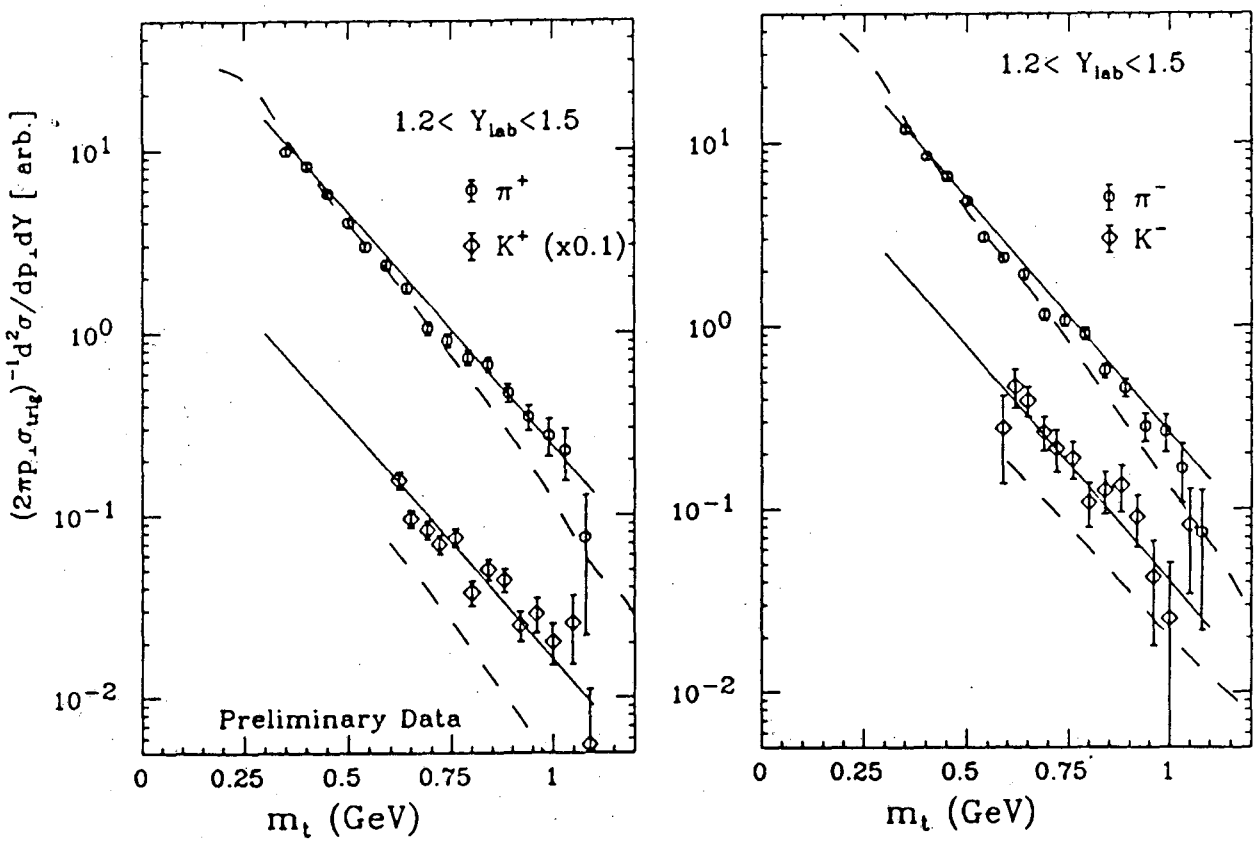
1.2< Y_lab<1.5
Φ π+
Φ K+ (x0.1)
Preliminary Data
(2πp⊥σ_tot)^-1 d²σ/dp⊥dY [arb.]
m_t (GeV)
1.2< Y_lab<1.5
Φ π-
Φ K-
m_t (GeV)

Fig. 9

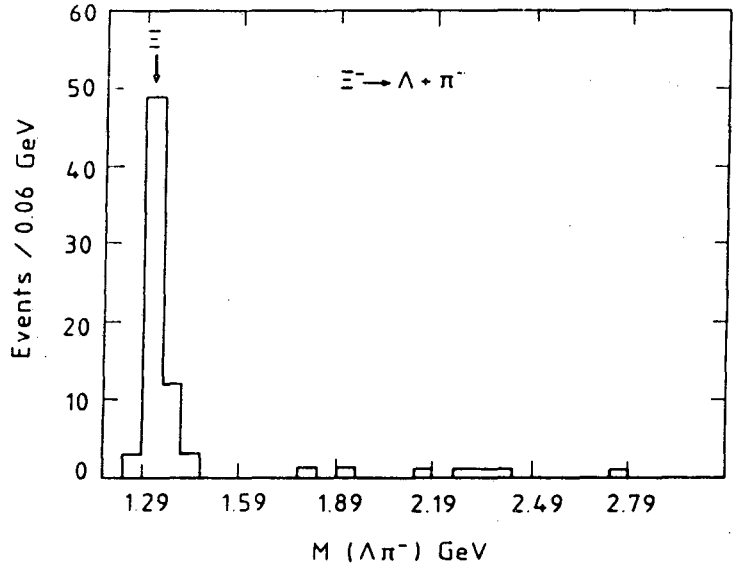
Ξ
Ξ⁻ → Λ + π⁻
Events / 0.06 GeV
M (Λπ⁻) GeV

Fig. 10

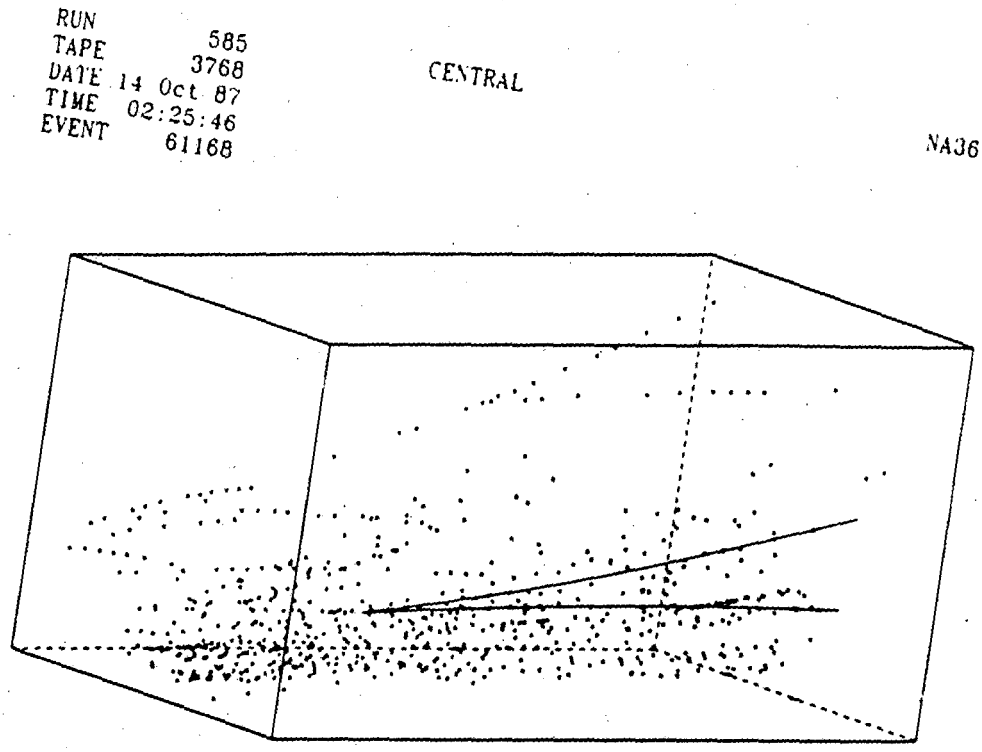
RUN 585
TAPE 3768
DATE 14 Oct 87
TIME 02:25:46
EVENT 61168
CENTRAL
NA36 TPC

Fig. 11

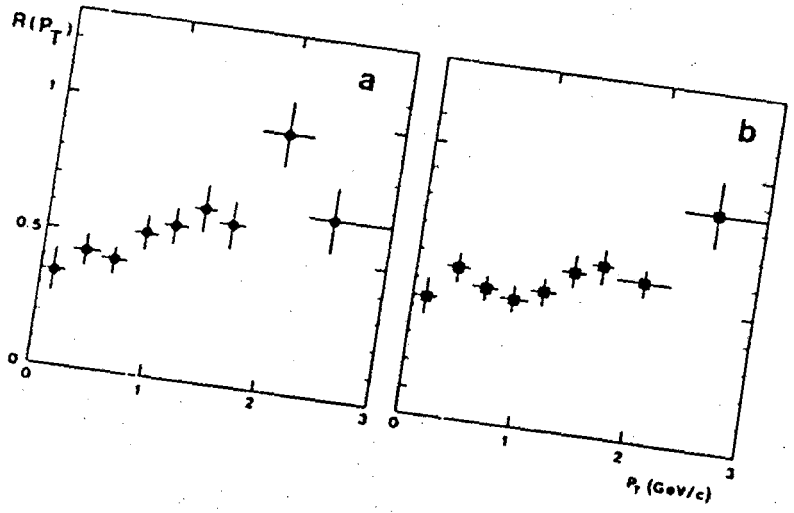
R(P_T)
a
b
1
0.5
0
0
1
2
3
P_T (GeV/c)

Fig. 12

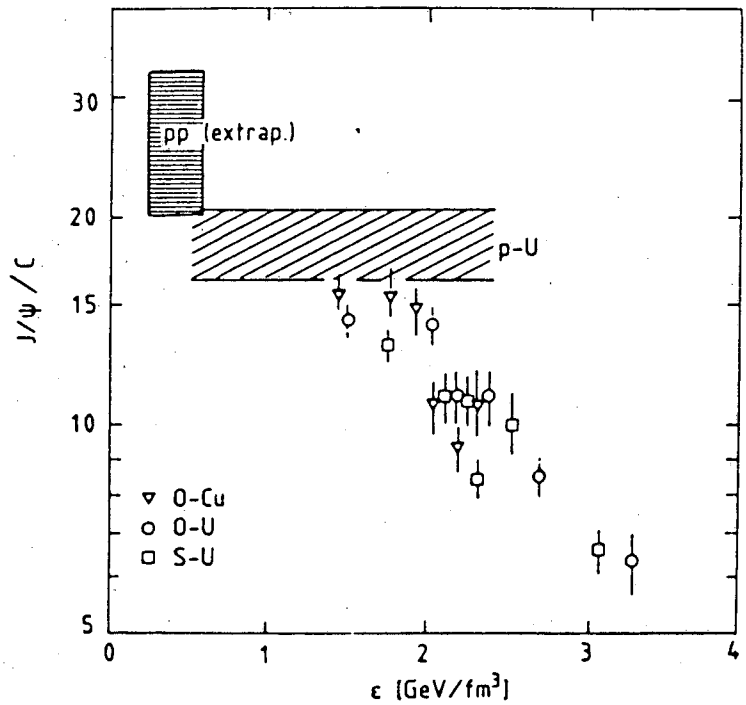
pp (extrap.)
p-U
O-Cu
O-U
S-U
J/ψ / C
ε [GeV/fm³]

Fig. 13

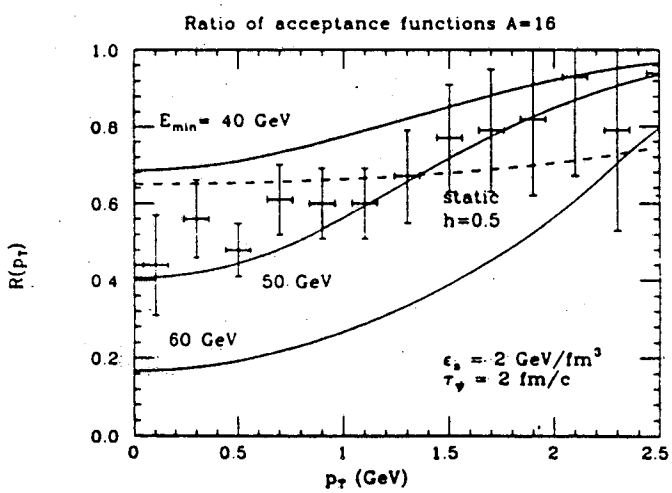
Ratio of acceptance functions A=16
E_min= 40 GeV
static
h=0.5
50 GeV
60 GeV
ε_s = 2 GeV/fm³
τ_ψ = 2 fm/c
R(p_T)
p_T (GeV)

Fig. 14

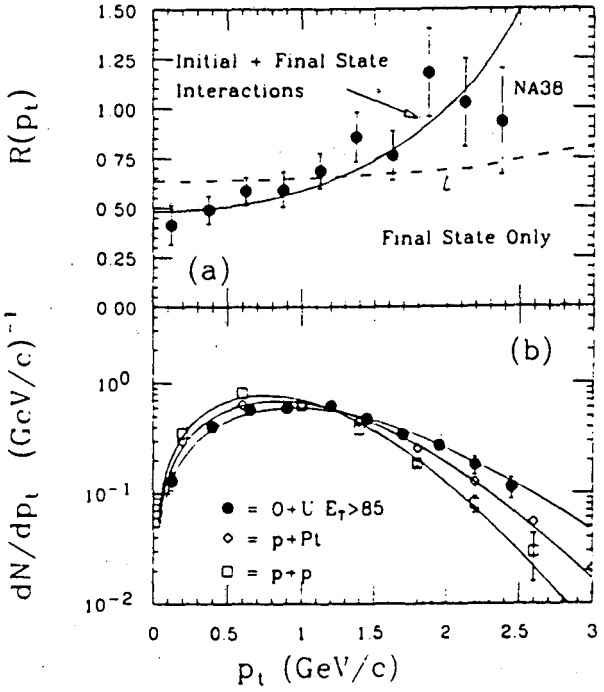
1.50
1.25
1.00
0.75
0.50
0.25
0.00
R(p_t)
Initial + Final State
Interactions
NA38
Final State Only
(a)
(b)
dN/dp_t (GeV/c)^-1
10^0
10^-1
10^-2
● = O+U E_T>85
◇ = p+Pt
□ = p+p
0
0.5
1
1.5
2
2.5
3
p_t (GeV/c)

Fig. 15

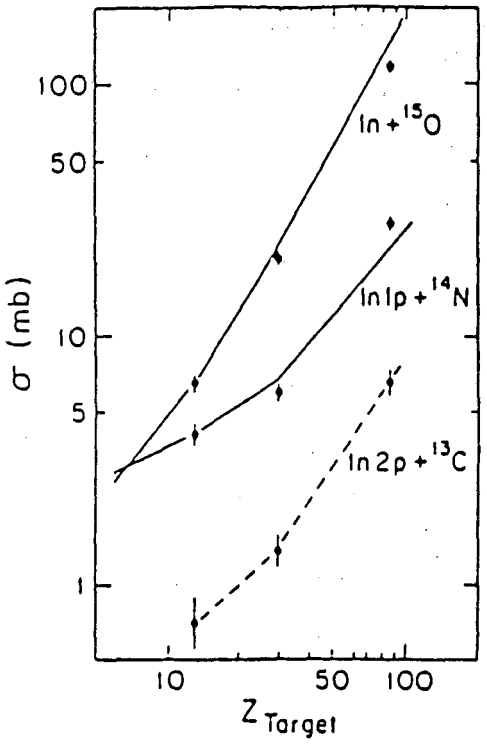
100
50
10
5
1
σ (mb)
In + ^15O
In Ip + ^14N
In 2p + ^13C
10
50
100
Z Target

Fig. 16

LAWRENCE BERKELEY LABORATORY
TECHNICAL INFORMATION DEPARTMENT
1 CYCLOTRON ROAD
BERKELEY, CALIFORNIA 94720